PTEP

Prog. Theor. Exp. Phys. **2017**, 043E01 (10 pages)
DOI: 10.1093/ptep/ptx037

A note on geodesics in the Hayward metric

Takeshi Chiba[1,*] and Masashi Kimura[2,*]

[1] *Department of Physics, College of Humanities and Sciences, Nihon University, Tokyo 156-8550, Japan*
[2] *CENTRA, Departamento de Fisica, Instituto Superior Tecnico-IST, Universidade de Lisboa-UL, Avenida Rovisco Pais 1, 1049 Lisboa, Portugal*
[*] E-mail: chiba@phys.chs.nihon-u.ac.jp, masashi.kimura@tecnico.ulisboa.pt

Received January 30, 2017; Accepted March 2, 2017; Published April 12, 2017

We study timelike and null geodesics in a nonsingular black hole metric proposed by Hayward. The metric contains an additional length-scale parameter ℓ and approaches the Schwarzschild metric at large radii while it approaches a constant at small radii so that the singularity is resolved. We tabulate the various critical values of ℓ for timelike and null geodesics: the critical values for the existence of horizon, marginally stable circular orbit, and photon sphere. We find the photon sphere exists even if the horizon is absent and two marginally stable circular orbits appear if the photon sphere is absent and a stable circular orbit for photons exists for a certain range of ℓ. We visualize the image of a black hole and find that blight rings appear even if the photon sphere is absent.

Subject Index E00

1. Introduction

A nonsingular model of a black hole was proposed by Hayward (Ref. [1]). As such, it may be a solution of an ultraviolet complete gravity such as Refs. [2,3]. The geodesics in such a nonsingular spacetime would illuminate some basics aspects of the spacetime, as the geodesics in the Schwarzschild spacetime do (Ref. [4]).

In this paper, we summarize the results of our study of the properties of geodesics in the geometry described by the Hayward metric, in a self-contained manner. Some of the results may be already known (e.g., Refs. [5,6]), but the detailed study of both the properties of marginally stable circular orbits and the behavior of null geodesics are new as far as we know.

In Sect. 2, after giving the radii of the horizons of the spacetime, we study the properties of timelike geodesics and null geodesics. Section 3 is devoted to a summary. In Appendix, we summarize the properties of the geodesics in the Reissner–Nordström metric.

We use the units of $G = c = 1$.

2. Geodesics in the Hayward metric

The Hayward metric is given by (Ref. [1])

$$ds^2 = -F(r)\,dt^2 + \frac{dr^2}{F(r)} + r^2 d\Omega^2, \qquad F(r) = 1 - \frac{2Mr^2}{r^3 + 2\ell^2 M}, \tag{1}$$

where M is a mass parameter and ℓ is a length-scale parameter. The metric approaches $1 - 2M/r$ as $r \to \infty$ and approaches unity smoothly as $r \to 0$ and hence is nonsingular. The metric is "minimal" in the sense that it contains the least number of free parameters (ℓ only) with the desired properties (regularity at the center such that $F(r) \to 1 + \mathcal{O}(r^2)$ and Schwarzschild asymptotic behavior at large radii). In fact, Frolov has recently shown that if $F(r)$ is a rational function of r, the order of the polynomials must be larger than 2 and an $F(r)$ that is constructed out of polynomials of order 3 contains two free parameters in general (Ref. [7]).

We may compute the effective energy momentum for the metric (1) via $T_{\mu\nu} = \frac{1}{8\pi} G_{\mu\nu}$ as done in Ref. [1]. Then, the energy density $\rho = -T^t{}_t$, the radial pressure $p_r = T^r{}_r$, and the tangential pressure $p_T = T^\theta{}_\theta = T^\phi{}_\phi$ are given by (Ref. [1])

$$\rho = -p_r = \frac{3\ell^2 M^2}{2\pi(r^3 + 2\ell^2 M)^2}, \tag{2}$$

$$p_T = \frac{3\ell^2 M^2 (r^3 - \ell^2 M)}{\pi(r^3 + 2\ell^2 M)^3}, \tag{3}$$

and we find that the weak energy condition is satisfied: $\rho > 0$, $\rho + p_r = 0$, $\rho + p_T \geq 0$ and that the strong energy condition is violated for $r < (\ell^2 M)^{1/3}$ since $\rho + p_r + 2p_T = 2p_T$.

Henceforth, we normalize the length scale by M and introduce the dimensionless parameter

$$a \equiv \frac{\ell}{M}, \tag{4}$$

and use $\widetilde{r} = r/M$ as a dimensionless variable.

2.1. *Horizon*

The location of a horizon is determined by $F(r) = 0$, and horizons (outer horizon $\widetilde{r}_+$ and inner horizon $\widetilde{r}_-$) exist for $0 \leq a \leq a_{\rm H}$ (Ref. [1]):

$$\widetilde{r}_+ = \frac{2}{3} + \frac{4}{3}\cos\left(\frac{1}{3}\cos^{-1}\left(1 - \frac{27a^2}{8}\right)\right), \tag{5}$$

$$\widetilde{r}_- = \frac{2}{3} - \frac{4}{3}\cos\left(\frac{1}{3}\cos^{-1}\left(1 - \frac{27a^2}{8}\right) + \frac{\pi}{3}\right), \tag{6}$$

where

$$a_{\rm H} = \frac{4}{3\sqrt{3}} = 0.7698\ldots. \tag{7}$$

The upper bound on a implies the lower bound on M: $M \geq a_{\rm H}\ell$. The implications of this lower bound on the formation and the evaporation of black holes are discussed in Ref. [1]. In Fig. 1, we show the radii of the horizons (black curve). The causal structure is quite similar to the Reissner–Nordström black hole: $a < a_{\rm H}$, $a = a_{\rm H}$, $a > a_{\rm H}$ corresponds, respectively, to $Q < M$, $Q = M$, $Q > M$ for the Reissner–Nordström black hole, the only exception being that the central singularity is replaced with a regular center.

2.2. *Timelike geodesics*

From the spherical symmetry, we may restrict ourselves to the equatorial plane without loss of generality. In terms of two conserved quantities, the energy $E = F(r)\dot{t}$ and the angular momentum $L = r^2\dot{\phi}$, the timelike geodesics satisfy the energy equation

$$\frac{1}{2}\dot{r}^2 + V(r) = \frac{1}{2}E^2, \qquad V(r) = \frac{1}{2}\left(1 + \frac{L^2}{r^2}\right)F(r), \tag{8}$$

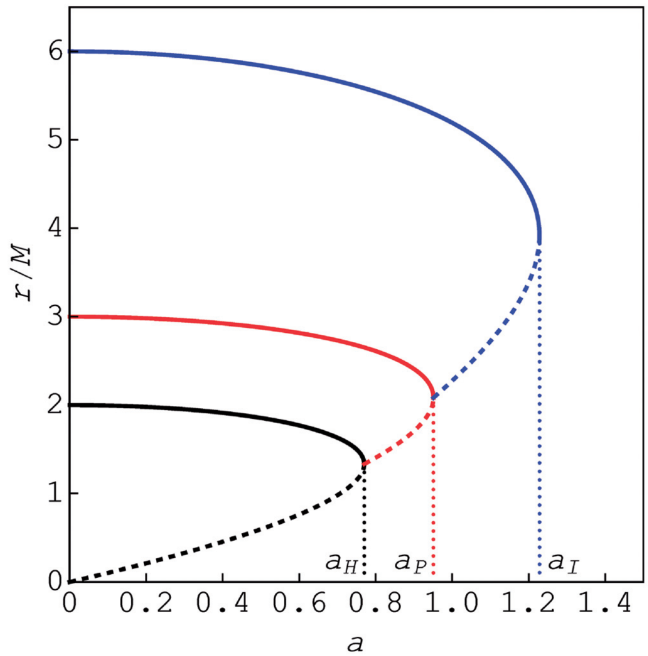

Fig. 1. The radii of horizons (black) (outer: solid; inner: dashed), ISCO or marginally stable circular orbit (blue), photon sphere (red solid) and stable circular orbit of photon (red dashed). Dotted vertical lines are critical values of $a = \ell/M$ (a_{H}, a_{P}, a_{I} from left).

where $\dot{t} = dt/d\tau$, with τ being the proper time.

A marginally stable circular orbit (MSCO) is determined by the condition $V' = V'' = 0$, which reduces to the following equation[1] for r:

$$\tilde{r}^6 - 6\tilde{r}^5 + 22a^2\tilde{r}^3 - 32a^4 = 0, \tag{9}$$

and the innermost such an orbit is called the innermost stable circular orbit (ISCO). Then, L^2 is determined by

$$\left(\frac{L}{M}\right)^2 = \frac{\tilde{r}^3\, dF/d\tilde{r}}{2F - \tilde{r}\, dF/d\tilde{r}} = \frac{\tilde{r}^7 - 4a^2\tilde{r}^4}{4a^4 + 4a^2\tilde{r}^3 + (\tilde{r} - 3)\tilde{r}^5}. \tag{10}$$

We find that Eq. (9) has one positive real solution for $a < a_{\mathrm{H}}$ and three positive real solutions for $a_{\mathrm{H}} < a < a_{\mathrm{I}}$ and one positive real solution for $a > a_{\mathrm{I}}$, where a_{I} is given by

$$a_{\mathrm{I}} = \frac{200}{51}\left(\frac{5}{51}\right)^{1/2} = 1.2278\ldots. \tag{11}$$

However, both of the solutions for $a_{\mathrm{H}} < a < a_{\mathrm{P}}$ and the single solution for $a > a_{\mathrm{P}}$ turn out to have imaginary L and are unphysical, where

$$a_{\mathrm{P}} = \frac{25}{24}\left(\frac{5}{6}\right)^{1/2} = 0.9509\ldots, \tag{12}$$

[1] If $F(r) = 1 - Q_{n-1}(r)/P_n(r)$, where $P_n(r)$ and $Q_{n-1}(r)$ are polynomials of order n and $n-1$, respectively, the degree of the equation becomes $3n - 3$.

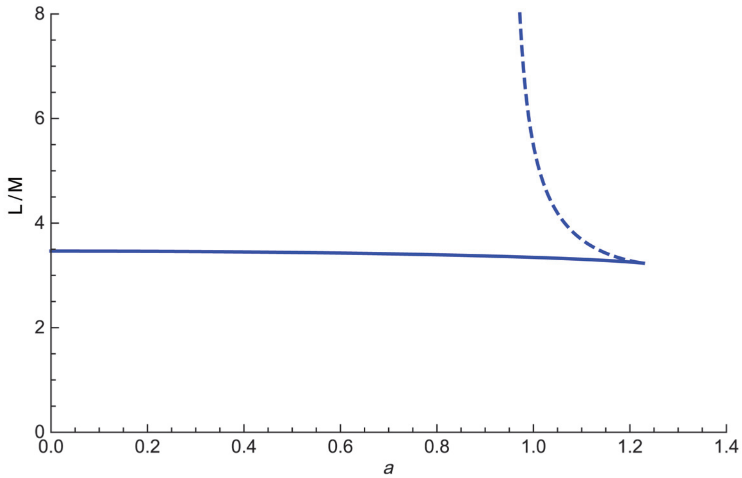

Fig. 2. The angular momentum of marginally stable circular orbits. The solid (respectively dashed) curve corresponds to the blue solid (respectively dashed) curve in Fig. 1.

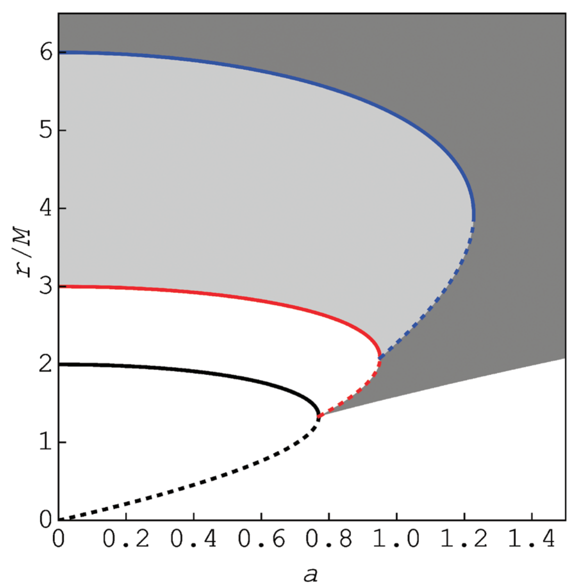

Fig. 3. The region of stable circular orbit (gray) as a function of a. The light gray region in the middle is the unstable orbit. The lower white region is forbidden because either the angular momentum is imaginary or the radius is inside the horizon. The blue (ISCO), red (photon sphere and circular null geodesics), and black (horizons) curves are the same as Fig. 1.

so there is no ISCO for $a > a_{\mathrm{I}}$. However, there is one ISCO for $a < a_{\mathrm{P}}$ and two MSCOs for $a_{\mathrm{P}} < a < a_{\mathrm{I}}$ and no ISCO for $a > a_{\mathrm{I}}$. In Figs. 1 and 2, we show the radii of ISCO or MSCO (blue curve) and the angular momentum. The angular momentum of the inner MSCO for $a_{\mathrm{H}} < a < a_{\mathrm{I}}$ is arbitrarily large as $a \to a_{\mathrm{P}}$.

In Fig. 3, we show the allowed region for the stable circular orbit (gray). The light gray region in the middle is the unstable orbit $d^2V/dr^2 < 0$. The lower white region is forbidden because the angular momentum is imaginary or the radius is inside the horizon.

In order to study the properties of circular orbits, we calculate the energy of a particle in circular orbit as a function the radius for $a = 0.5, 0.9, 1$ as shown in Fig. 4. The extrema of the energy

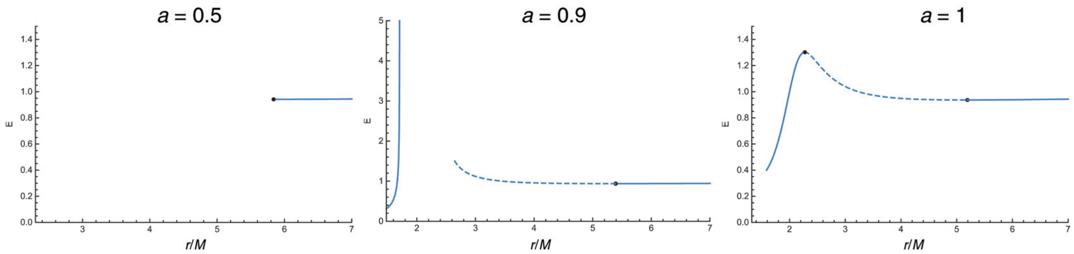

Fig. 4. The energy of a particle in circular orbit as a function of the radius of the orbit for $a = 0.5, 0.9, 1$ from left to right. The black dots correspond to marginally stable circular orbits. The circular orbit is unstable for the dashed curve.

correspond to MSCOs: for $a = 1$ the minimum is the outer MSCO and the maximum is the inner MSCO. The region in between two MSCOs (dashed curve) is unstable because $d^2V/dr^2 < 0$ there. The outer MSCO can be reached from a particle in circular orbit outside by its emitting energy and angular momentum. On the other hand, since the energy of the inner MSCO is larger than 1 (the energy at large r), the inner MSCO is unbounded and may be regarded as an "excited state" that cannot be reached from a particle in circular orbit outside. In this sense, only the outer MSCO may be physically important. For $a = 0.9$, there is also a stable circular orbit with large L and $E > 1$.

2.3. *Null geodesics*

As in the case of the timelike geodesics, in terms of E and L, the null geodesics satisfy

$$\frac{1}{2}\dot{r}^2 + V_{\rm null}(r) = \frac{1}{2}E^2, \qquad V_{\rm null}(r) = \frac{L^2}{2r^2}F(r), \tag{13}$$

where $\dot{r} = dr/d\lambda$ with λ being the affine parameter.

Since L/E is the impact parameter at large r, the (local) maximum of the effective potential $V_{\rm null}(r)$ determines the capture cross section for photons and hence the size of the shadow of a black hole: photons with a smaller impact parameter will be captured by the black hole. The location of the (local) maximum of $V_{\rm null}(r)$, or the radius of unstable circular orbits of photons (photon sphere, Ref. [8]), $r_{\rm P}$, is determined by

$$\widetilde{r}^6 - 3\widetilde{r}^5 + 4a^2\widetilde{r}^3 + 4a^4 = 0. \tag{14}$$

Similarly to the case of ISCO, we find that the maximum of $V_{\rm null}(r)$ exists if $a < a_{\rm P}$, where $a_{\rm P}$ is defined in Eq. (12). In Fig. 1 we show the radius of the photon sphere (red solid). There also appears a stable circular orbit of photon (red dashed) for $a < a_{\rm P}$. The appearance of a stable circular photon orbit is inevitable in the presence[2] of the photon sphere (local maximum of $V_{\rm null}$) since $V_{\rm null}$ positively diverges as $r \to 0$. In Fig. 5, we show the radius of the shadow $b_{\rm P}$ defined by

$$b_{\rm P} = \left(\frac{L^2}{2V_{\rm null}(r_{\rm P})}\right)^{1/2} = \frac{r_{\rm P}}{(F(r_{\rm P}))^{1/2}}. \tag{15}$$

In order to study the effect of the geometry on the propagation of light rays, we first compute the deflection of light in the Hayward metric. We consider the deflection of light in the equatorial plane.

[2] The presence of a stable photon orbit, however, would be problematic because perturbations can become long-lived and nonlinear effects may destabilize the system (Ref. [9]).

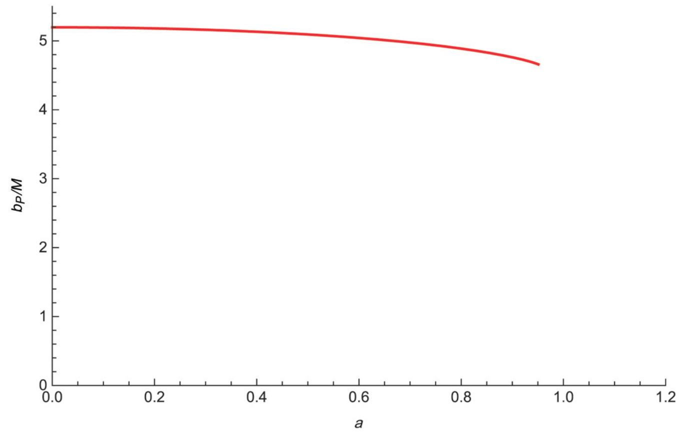

Fig. 5. Shadow radius b_{P} as a function of $a = \ell/M$.

Then from Eq. (13) and $L = r^2\dot{\phi}$, in terms of the impact parameter $b = L/E$, up to the turning point of the deflection, ϕ satisfies

$$r^2 \frac{d\phi}{dr} = \left(b^{-2} - \frac{F(r)}{r^2}\right)^{-1/2}. \tag{16}$$

Denoting the turning point of the deflection by r_0 at which $V_{\mathrm{null}}(r_0) = E^2/2$ or $b^{-2} = F(r_0)/r_0^2$, the deflection angle $\Delta\phi$ is then given by

$$\Delta\phi = 2\int_0^{1/r_0} \frac{du}{\left(b^{-2} - u^2 F(1/u)\right)^{1/2}} - \pi, \tag{17}$$

where we have made the change of variables $u = 1/r$ as usual. Expanding in terms of M/r_0 under the assumption $\Delta\phi$ is small (weak deflection), the result is

$$\begin{aligned}\Delta\phi = {} & \frac{4M}{r_0} + \frac{(15\pi - 16)}{4}\left(\frac{M}{r_0}\right)^2 + \frac{(244 - 45\pi)}{6}\left(\frac{M}{r_0}\right)^3 \\ & + \left(-130 + \frac{3465\pi}{64} - \frac{15\pi}{4}a^2\right)\left(\frac{M}{r_0}\right)^4 \\ & + \left(\frac{7783}{10} - \frac{3465\pi}{16} + \frac{75\pi - 472}{5}a^2\right)\left(\frac{M}{r_0}\right)^5 \\ & + \left(\frac{310\,695\pi}{256} - \frac{21397}{6} + \frac{5}{16}(1664 - 693\pi)a^2\right)\left(\frac{M}{r_0}\right)^6 + O\left(\left(\frac{M}{r_0}\right)^7\right).\end{aligned} \tag{18}$$

We show the result only up to $O((M/r_0)^6)$, although we can calculate arbitrarily higher orders. The coefficients for $a = 0$ fully agree with Ref. [10], but the sign of the coefficient of $(M/r_0)^4$ including a is different from Ref. [5] in which only the numerical values of the coefficient are given and higher-order terms are not given. In terms of the impact parameter b, using $b^{-2} = F(r_0)/r_0^2$, the deflection angle up to $O((M/b)^6)$ is given by

$$\Delta\phi = \frac{4M}{b} + \frac{15\pi}{4}\left(\frac{M}{b}\right)^2 + \frac{128}{3}\left(\frac{M}{b}\right)^3 + \left(\frac{3465\pi}{64} - \frac{15\pi}{4}a^2\right)\left(\frac{M}{b}\right)^4$$

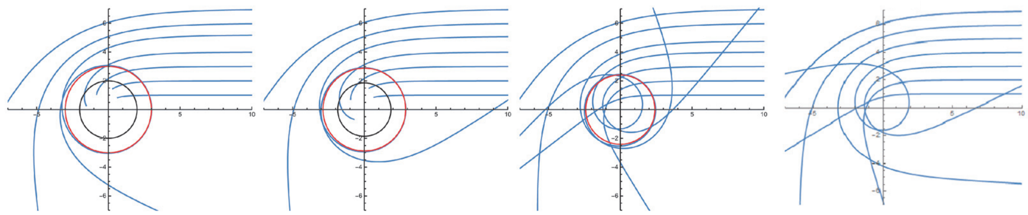

Fig. 6. Trajectories of light rays (coming in from upper right) for $a = 0, 0.5, 0.9, 1$ from left to right. The black circles are the (outer) horizon, the red circles are the radii of photon spheres.

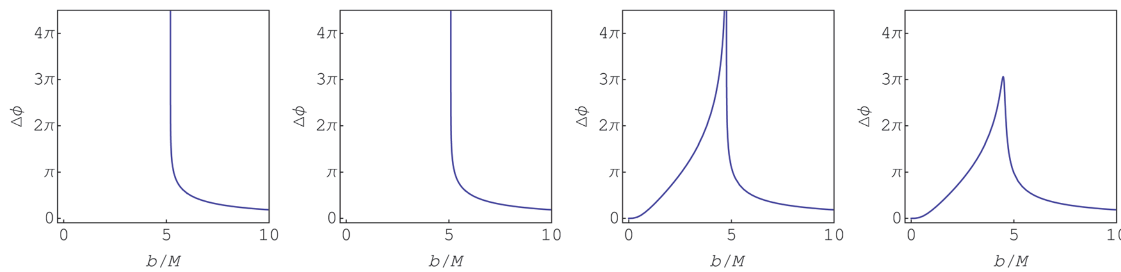

Fig. 7. The deflection angle as a function of the impact parameter b for $a = 0, 0.5, 0.9, 1$ from left to right.

$$+\left(\frac{3584}{5}-\frac{512a^2}{5}\right)\left(\frac{M}{b}\right)^5+\left(\frac{255\,255\pi}{256}-\frac{3465\pi}{16}a^2\right)\left(\frac{M}{b}\right)^6$$
$$+O\left(\left(\frac{M}{b}\right)^7\right). \tag{19}$$

Again, we find complete agreement with Ref. [10] up to this order if $a = 0$. Since the effect of nonzero a appears only for $O((M/b)^4)$ and beyond, it is difficult to detect the effect of the (weak) deflection angle. From the requirement that the fourth term should not exceed the 0.001% of the first term (Ref. [11]), a is constrained only as $a \lesssim 10^5(b/R_\odot)^{3/2}(M/M_\odot)^{-3/2}$ or $\ell \lesssim 10^5\,\mathrm{km}(b/R_\odot)^{3/2}(M/M_\odot)^{-1/2}$.

However, the presence of a does affect the existence or nonexistence of the photon sphere and hence affects the behavior of light rays traveling around the photon sphere. In Fig. 6, we show the trajectories of light rays coming in from the upper right for $a = 0, 0.5, 0.9, 1$. The black circle is the (outer) horizon, and red circles are the radii of photon spheres. In Fig. 7, we show the deflection angle as a function of the impact parameter b for $a = 0, 0.5, 0.9, 1$. If the impact parameter is slightly larger than the radius of a shadow b_{P}, the deflection angle $\Delta\phi$ is logarithmically divergent as

$$\Delta\phi \sim \frac{1}{\left(-5+2\,(3r_{\mathrm{P}}/M)^{1/2}\right)^{1/2}}\ln(b-b_{\mathrm{P}})^{-1}. \tag{20}$$

If $a = a_{\mathrm{P}}$, i.e., $r_{\mathrm{P}} = 25/12$, the divergent behavior is changed into

$$\Delta\phi \sim c_0 M^{1/6}(b-b_{\mathrm{P}})^{-1/6}, \tag{21}$$

$$c_0 = 2^{11/6}3^{2/3}5^{5/4}\int_0^\infty dy\frac{1}{\left(432y+900y^2+625y^3\right)^{1/2}} \simeq 7.771. \tag{22}$$

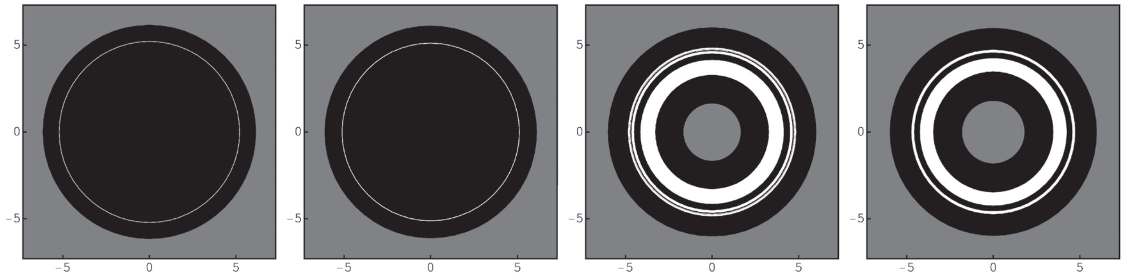

Fig. 8. Image of a nonsingular black hole described by the Hayward metric for $a = 0, 0.5, 0.9, 1$ from left to right. Photons in black regions never reach the observer. Photons in white regions travel around the central region more than once, while photons in gray regions reach the observer straightforwardly.

Quite similar behavior is also found for the Reissner–Nordström metric, where critical values corresponding to $a_{\rm H}$, $a_{\rm P}$ appear depending on the value of the charge (Appendix).

The images of a "black hole" are shown in Fig. 8. Photons in black regions never reach the observer due to the presence of a horizon or the deflection angle being $\pm\pi/2$ (modulo 2π). Photons in white regions travel around the central region more than once, while photons in gray regions reach the observer straightforwardly. The image for $a = 0.5$ is little different from that of a Schwarzschild black hole ($a = 0$): A blight ring surrounding a black disk (shadow of a black hole) appears. Interestingly, for $a = 0.9$ ($a_{\rm H} < a < a_{\rm P}$), the photon sphere exists even though the horizon is absent; a black disk disappears and a black doughnut appears instead, and a ring image persists. More interestingly, even for $a = 1$ ($> a_{\rm P}$), the ring persists although the photon sphere is absent, as shown in Fig. 8. Therefore, the existence of a blight ring image does not necessarily imply the existence of a photon sphere. Of course, for astrophysical black holes $a \simeq 10^{-38}(\ell/\ell_{\rm p})(M_\odot/M) \ll 1$, where $\ell_{\rm p}$ is the Planck length, and these phenomena would be expected only for Planck-scale primordial black holes.

3. Summary

In this paper, we have studied the timelike and null geodesics in a nonsingular black hole geometry proposed by Hayward that involves a parameter ℓ, and found several interesting features of the geometry: the existence or nonexistence of the horizon, the photon sphere, and the ISCO. We also have found that two marginally stable circular orbits appear for $a_{\rm H} < \ell/M < a_{\rm P}$, although the inner orbit is unbound. The existence of a horizon and/or a photon sphere significantly affects the behavior of the null geodesics. We have found that a black doughnut appears if the horizon is absent and that blight rings appear even if the photon sphere is absent.

One may think that bright regions in a shadow image are due to the existence of the photon sphere. However, as shown in Fig. 8, bright regions also can appear in the spacetime with no photon sphere if the parameter a is slightly larger than $a_{\rm P}$. For such parameters, while there is no photon sphere, $\Delta\phi$ can still take a value larger than 2π (see Fig. 7). Similar behavior can be found in the Reissner–Nordström metric. These results suggest that such shadow images are universal behavior for parameters slightly larger than the critical value where photon sphere marginally exists. The parameter ℓ is currently only loosely constrained by the solar-system experiment since the deflection angle at the post-Newtonian order is the same as that of Schwarzschild. The Event Horizon Telescope, a long baseline interferometer experiment, will be able to resolve black holes at horizon scales with the angular resolution of 20 μas, which corresponds to a size of $3.6M$ for SgA* at the galactic center

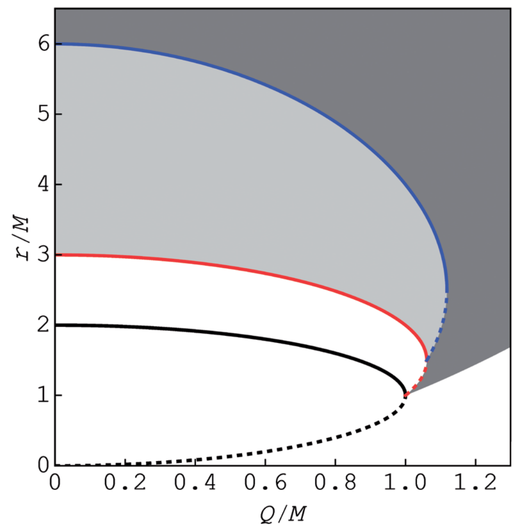

Fig. A1. The regions of stable and unstable circular orbits as a function of Q/M.

(Ref. [12]). If the shadow of a black hole is observed by such a telescope, we may put an $O(1)$ constraint on ℓ/M.

Acknowledgements

This work is supported by the MEXT Grant-in-Aid for Scientific Research on Innovative Areas (15H05894) and in part by Nihon University. M.K. acknowledges financial support provided under the European Union's H2020 ERC Consolidator Grant "Matter and strong-field gravity: New frontiers in Einstein's theory", grant agreement no. MaGRaTh-646597, and under the H2020-MSCA-RISE-2015 grant no. StronGrHEP-690904.

Appendix. Reissner–Nordström metric

The Reissner–Nordström metric is given by

$$ds^2 = -F(r)\,dt^2 + \frac{dr^2}{F(r)} + r^2\,d\Omega^2, \qquad F(r) = 1 - \frac{2M}{r} + \frac{Q^2}{r^2}, \tag{A1}$$

where M, Q are mass and electric charge parameters, respectively. We study the properties of geodesics on this metric and compare the result with the case of the Hayward metric.

Since the electric charge parameter appears in the metric as Q^2, we need to consider $Q \geq 0$ only. If $1 \geq Q/M$, there are two horizons at $r = r_\pm = M^2 \pm \left(M^2 - Q^2\right)^{1/2}$.

In Fig. A1, we have plotted the regions of stable and unstable circular orbits. The qualitative feature is the same as the case of the Hayward metric in Fig. 3. When Q/M takes the values $Q_{\rm H}/M = 1$, $Q_{\rm P}/M = 3/(2\sqrt{2}) \simeq 1.061$, and $Q_{\rm I}/M = \sqrt{5}/2 \simeq 1.118$, the horizon becomes extremal, the photon sphere marginally exists, and the ISCO marginally exists, respectively. The locations of the photon sphere and the shadow image for the Reissner–Nordström metric are also discussed in Ref. [13].

Figure A2 shows the deflection angle for null geodesics as a function of the impact parameter b. Compared to the case of the Hayward metric (see Fig. 7), the qualitative behavior is almost the same. The only difference can be found near the region for small impact parameter $b \simeq 0$ in overcharged cases $Q/M > 1$, where the deflection angle $\Delta\phi$ is almost $-\pi$. This is because the null geodesic is reflected by the repulsive force near the origin $r = 0$.

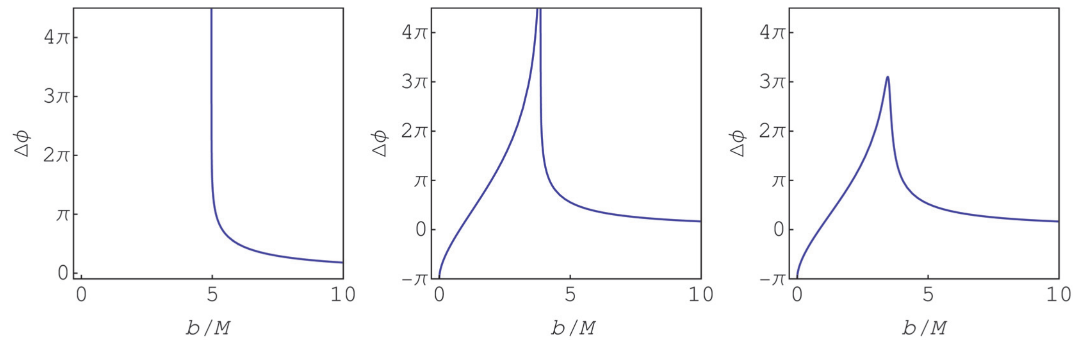

Fig. A2. The deflection angle as a function of the impact parameter b for $Q/M = 0.5$, 1.03, 1.08 from left to right.

If we consider $Q > Q_{\mathrm{P}}$, there is no photon sphere. However, for a parameter value slightly larger than Q_{P} (see the third figure in Fig. A2), $\Delta\phi$ can still take a value larger than 2π. This means that their shadow image is similar to the fourth figure in Fig. 8.

References

[1] S. A. Hayward, Phys. Rev. Lett. **96**, 031103 (2006) [arXiv:gr-qc/0506126] [Search INSPIRE].
[2] L. Modesto, Phys. Rev. D **86**, 044005 (2012) [arXiv:1107.2403 [hep-th]] [Search INSPIRE].
[3] T. Biswas, E. Gerwick, T. Koivisto, and A. Mazumdar, Phys. Rev. Lett. **108**, 031101 (2012) [arXiv:1110.5249 [gr-qc]] [Search INSPIRE].
[4] S. Chandrasekhar, *The Mathematical Theory of Black Holes* (Oxford University Press, Oxford, 1983).
[5] S. W. Wei, Y. X. Liu, and C. E. Fu, Adv. High Energy Phys. **2015**, 454217 (2015) [arXiv:1510.02560 [gr-qc]] [Search INSPIRE].
[6] J. Schee and Z. Stuchlik, J. Cosmol. Astropart. Phys. **1506**, 048 (2015) [arXiv:1501.00835 [astro-ph.HE]] [Search INSPIRE].
[7] V. P. Frolov, Phys. Rev. D **94**, 104056 (2016) [arXiv:1609.01758 [gr-qc]] [Search INSPIRE].
[8] K. S. Virbhadra and G. F. R. Ellis, Phys. Rev. D **62**, 084003 (2000) [arXiv:astro-ph/9904193] [Search INSPIRE].
[9] V. Cardoso, L. C. B. Crispino, C. F. B. Macedo, H. Okawa, and P. Pani, Phys. Rev. D **90**, 044069 (2014) [arXiv:1406.5510 [gr-qc]] [Search INSPIRE].
[10] C. R. Keeton and A. O. Petters, Phys. Rev. D **72**, 104006 (2005) [arXiv:gr-qc/0511019] [Search INSPIRE].
[11] B. Bertotti, L. Iess, and P. Tortora, Nature **425**, 374 (2003).
[12] S. Doeleman et al., Nature **455**, 78 (2008) [arXiv:0809.2442 [astro-ph]] [Search INSPIRE].
[13] A. F. Zakharov, Phys. Rev. D **90**, 062007 (2014) [arXiv:1407.7457 [gr-qc]] [Search INSPIRE].